GUIDANCE, AVIONICS AND NAVIGATION SYSTEM OF AN AUTONOMOUS AIRSHIP FOR DEMINING

Ricardo Coutinho do Valle
Brazilian Army Technological Center, 28705, Rio de Janeiro, RJ, 23020-470, Brazil
ricardovalle@ctex.eb.br

Luciano Luporini Menegaldo
Federal University of Rio de Janeiro, Rio de Janeiro, RJ, 21941-914, Brazil
lmeneg@ufrj.br

Alberto Mota Simões
Military Institute of Engineering, Rio de Janeiro, RJ, 22290-270, Brazil
simoes@ime.eb.br

Abstract. *During demining operations, the increasing international demands for safety, accuracy and productivity suggests the use of autonomous aircraft, primarily in detection phase. Among the possible platforms, airships have advantages in covering large areas with relatively low operating costs. An autonomous flight system for this task requires carefully designed open-loop and feedback control systems, for sweeping the target area and compensate for atmospheric disturbances. Control algorithms, sensor data recording and actuator drivers, as well as the communications with the land basis, require a set of hardware, firmware and software devices, which must be suitably integrated. This paper presents the integrated avionics and the navigation system of an Autonomous Sweeping Airship for Demining (ASAD), as well as the general laws of guidance and control systems. The main avionics system consists of a dsPIC processor, three-axis Inertial Measurement Unit, GPS receiver, three-axis magnetometer and a barometric sensor. Guidance simulations and inertial data obtained by a sensor are shown, demonstrating the feasibility of using the presented guidance and navigation system.*

Keywords: *UAV, demining, airship, navigation, avionics.*

1. INTRODUCTION

Unmanned Aircraft Systems (UAS) have been increasingly used in many tasks that may become dangerous to humans but also require accuracy. An application example is in the field of demining and anti-terrorism actions, where Unmanned Aerial Vehicles (UAV) play a relevant role. The demand for UAV in demining operations is caused, among others, by two main factors. First, the global problem of demining. Minefields are present in some 90 countries, totaling an estimated 45 to 50 million anti-personnel landmines still installed in the world. Mines have low cost and, once installed, remain active for decades (Daniels, 2006). Annually, around 1.9 million new mines are installed, against a removal rate of 100,000 mines (MacDonald and Lockwood, 2003). All these features make mines cause a large number of deaths and mutilations, being mostly civilians in the post-conflict period. The second motivation is the minefields disposal, which normally scattered over large areas with few or without any information from conflict time.

In minefield detections, several kinds of sensor technologies have been used alone or gathered, such as ultra wideband radar (UWB) (Bishop *et al.*, 1998), ground penetrating radar (GPR) (Cross and Osborn, 2010) and infrared detection (Meurer *et al.*, 2010). To perform coverage and scanning large areas, airships have some advantages, namely hovering or fly at low speeds (Khoury and Gillett, 1999), low costs (Frye *et al.*, 2007) and show extended flight endurance under favorable climate conditions. Airships also can be used as test platforms containing sensors for data fusion, reducing costs in the early stages of systems design, until the final aircraft project is consolidated.

In the past years, a relevant amount of works have been dedicated to solve airship tasks and its applications. Most of the literature in airship dynamics and design started from 1920s, presenting the aerodynamic forces on airships (Munk, 1922), the factors of apparent additional mass (Munk, 1924), the structural problem (Burgess, 1927), aerodynamics theory of airships (Munk, 1936), and their fluid-dynamic influences (Lamb, 1945; Allen and Perkins, 1951; Hoerner, 1958). The modeling of large airships has been consolidated through works like (Gomes and Ramos , 1998; Li and Nahon , 2007; Li , 2008; Li *et al.*, 2011), as well the dynamic of small highly maneuverable airships (Nong , 2012). The influences of wind disturbances on airship dynamics is investigated in (Thomasson , 2000; Azinheira *et al.*, 2002, 2008). In the field of linear approach, attitude (Paiva *et al.*, 1999; Azinheira *et al.*, 2001; Paiva *et al.*, 2001) and velocity control (Wimmer and Well , 2001) are treated by techniques like PID (Earon *et al.*, 2007; Peddiraju , 2010; Ramos *et al.*, 2001; Paiva *et al.*, 2006), LQR (Kulczycki *et al.*, 2006; Silveira *et al.*, 2002), H_∞ (Elfes *et al.*, 2003; Azinheira *et al.*, 2000; Liesk , 2012) and nonsmooth multi-objective synthesis (do Valle *et al.*, 2012). Likewise, solutions using nonlinear control approaches

are present through methods like input-output linearization and Lyapunov (Liang and Xiong , 2006), as well backstepping (Azinheira *et al.*, 2006). Additionally, other path tracking solutions are addressed by Lyapunov theory (Zhang *et al.*, 2008), backstepping (Repoulias and Papadopoulos , 2008), and spatial vectors method (Adamski *et al.*, 2010).

This work is a portion of the study efforts in order to develop an Autonomous Sweeping Airship for Demining (ASAD), which can board one or more detection sensors and perform minefields sweeping. To define the navigation path and define avionics requirements, the dynamics of ASAD as well as general guidance and control laws are presented, taking into account atmosphere disturbances (McLean, 1990).

The high accuracy of UAV flight depends substantially on navigation data. The solution combining strapdown inertial navigation system (INS), global positioning system (GPS) and barometer integrated system can provide higher navigation performance (Jiong *et al.*, 2010), (Huang and Fang, 2005). Both have been included in the present project.

This work presents the main avionics system embedded into an airship with demining purposes. The modeling is briefly addressed as well as the control solution, tested against possible disturbances patterns. The general guidance law is also addressed. Finally, some results from simulations as well as one data experiment with a sensor are presented.

2. MODELING, GENERAL GUIDANCE AND CONTROL LAWS

The modeling is applied to an airship with a propulsion system consisting of three electric motors coupled to helices and without any vectoring capability. Two of them are oriented parallel to the longitudinal axis, spaced laterally by $1m$. The third engine is placed such that its propulsion force is perpendicular to the airship lateral plane, providing a lift augmentation that is convenient to improve low-speed controllability. All of the three motors can provide bi-directional forces. On the other hand, there is no aerodynamic control surfaces. Therefore, in open loop, control inputs consisted only in propulsion forces (do Valle *et al.*, 2012). The envelope is considered as a double-ellipsoid shape (Mueller *et al.*, 2004) with 17.54 m^3. The airship contains four stabilizers arranged in a cross shape and its main characteristics is shown in Tab. 1.

Table 1. Airship main physical characteristics

Description [$Units$]	Value
Semi-major axis 1 [m]	2.17
Semi-major axis 2 [m]	4.53
Semi-minor axis [m]	1.12
x-component of center of gravity [m]	0.18
z-component of center of gravity [m]	0.74
Carriage and systems mass [kg]	16.33
Envelope and fins mass [kg]	5.16
Moments of inertia about the X axis [$kg.m^2$]	25.26
Moments of inertia about the Y axis [$kg.m^2$]	50.29
Moments of inertia about the Z axis [$kg.m^2$]	31.33
Products of Inertia about OY [$kg.m^2$]	0.16

A non-linear 6-DOF rigid body model is assumed, with same parameters presented in (do Valle *et al.*, 2012):

$$\begin{bmatrix} \dot{U} \\ \dot{V} \\ \dot{W} \\ \dot{p} \\ \dot{q} \\ \dot{r} \end{bmatrix} = M^{-1}\left(F_d + A_{\alpha\beta} + G + P\right) \tag{1}$$

where $\dot{U}$, $\dot{V}$, $\dot{W}$ are the derivatives of translational velocity components in body frame reference system and $\dot{p}$, $\dot{q}$, $\dot{r}$ are the derivatives of angular velocities as can be seen in Fig. 1.

The components presented at right-hand of Eq. (1) represent (Kulczycki *et al.*, 2008):

M: the system mass and inertia matrices, including the added mass and inertia;

F_d: vector containing the centrifugal and Coriolis force and moment components;

$A_{\alpha\beta}$: the aerodynamic force vector, which depends on attack (α) and sideslip (β) angles;

G: forces and moments components due to weight and buoyancy; and

P: the propulsion vector containing components of thrust;

All these terms are computed as in (do Valle *et al.*, 2012).

The atmospheric disturbances include constant winds incidence and turbulent gusts (McLean, 1990). The effects of

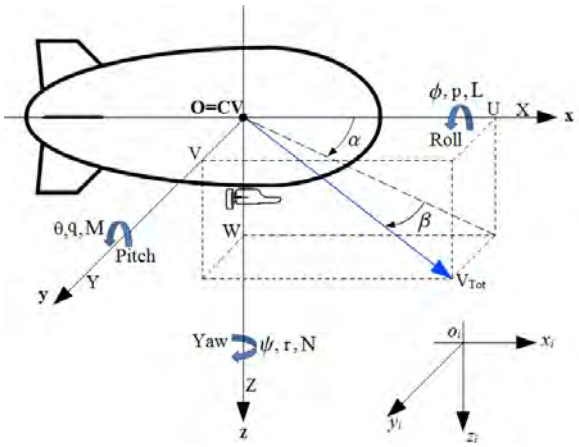

Figure 1. Airship reference systems (body fixed - $oxyz$ and inertial - $o_i x_i y_i z_i$).

atmospheric disturbances are included within the aerodynamic forces, considering the total linear speed used in aerodynamic computations, as the relative velocity of the aircraft with respect to the air flow generated by wind and gusts. Than linearized model is expressed as (Paiva *et al.*, 2006):

$$\dot{x} = Ax + Bu + Ed \tag{2}$$

where x are space states, u is the control input, d is the disturbance input, and A, B, and E are the state-space matrices found at the trim point chosen. Trimming condition corresponds to the aircraft in equilibrium condition, i.e., flying at constant speed without any wind incidence.

2.1 General Equations and Control Law

The whole dynamics state vector is defined in Eq. (3), containing the usual decoupled longitudinal and lateral systems components plus yaw angle for guidance and control purposes, as shown bellow:

$$x = \begin{bmatrix} U & V & W & p & q & r & \phi & \theta & \psi \end{bmatrix}^T \tag{3}$$

The main kinematic equations in the inertial reference frame are (Wang *et al.*, 2010):

$$\dot{x} = (\cos\psi\cos\theta)U + (\cos\psi\sin\theta\sin\phi - \sin\psi\cos\phi)V + (\cos\psi\sin\theta\cos\phi + \sin\psi\sin\phi)W \tag{4}$$

$$\dot{y} = (\sin\psi\cos\theta)U + (\sin\psi\sin\theta\sin\phi + \cos\psi\cos\phi)V + (\sin\psi\sin\theta\cos\phi - \cos\psi\sin\phi)W \tag{5}$$

$$\dot{h} = -\dot{z} = (\sin\theta)U - (\cos\theta\sin\phi)V - (\cos\theta\cos\phi)W \tag{6}$$

where $\dot{x}$, $\dot{y}$, $\dot{h}$ are the inertial velocity components and ϕ, θ, ψ the Euler angles. A relationship between angular velocities p, q, r of the aircraft fixed axes, with respect to angular components of velocity $\dot{\phi}$, $\dot{\theta}$ and $\dot{\psi}$, in inertial frame follows:

$$\begin{aligned} p &= \dot{\phi} - \dot{\psi}\sin\theta \\ q &= \dot{\theta}\cos\phi + \dot{\psi}\sin\phi\cos\theta \\ r &= \dot{\psi}\cos\phi\cos\theta - \dot{\theta}\sin\phi \end{aligned} \tag{7}$$

The complete control block diagram is shown in Fig. 2,where the gain matrices K_i and K_x represent the design variables to be determined by the control synthesis method. The overall control of the airship in terms of input references is done through that diagram. Control vector u_c correspond the thrust forces T_1, T_2 e T_3 delivered by each motor. The input vector r_o contains u_r, w_r, and ψ_r, respectively, references for linear velocities in body frame at x and w directions and yaw angle.

Given the diagram presented in Fig. 2, two different controllers synthesis solution have been tested. The first was a full-state feedback Linear Quadratic Regulator (LQR) and latter, multi-objective control design method based on nonsmooth optimization (Simões *et al.*, 2009). For ASAD application, the main advantages of multi-objective synthesis are the possibility to directly address time-domain constrains in the control synthesis, as well as closed loop spectral damping constraints.

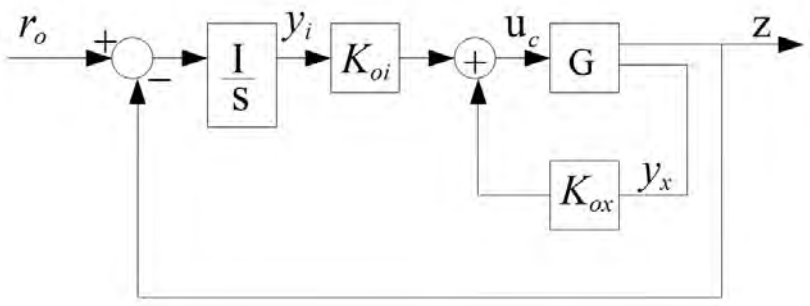

Figure 2. ASAD Control Architeture.

2.2 Guidance Law

The airship is assumed as a geometric point $P_A = [x_A \quad y_A \quad z_A]^T$ in the inertial reference frame (Lin, 1991), that must arrive into a homing point $P_O = [x_O \quad y_O \quad z_O]^T$. A directional vector is given by:

$$\vec{D} = \vec{P}_O - \vec{P}_A \tag{8}$$

where the next waypoint $\vec{P}_O$ in the trajectory and the absolute closing velocity V_c are given by a path determiner block shown in Fig. 5. Likewise the points P_A and P_O, the closing velocity is referenced in the inertial frame.

Assuming that the aircraft is in homing course with velocity V_c, the time to go (t_g) is found from:

$$t_g = \frac{\left|\vec{D}\right|}{\left|\vec{V}_c\right|} \tag{9}$$

The linear velocities in the inertial reference frame (North-East-Down) are given by:

$$V_x = \frac{x_O - x_A}{t_g} \quad ; \quad V_y = \frac{y_O - y_A}{t_g} \quad ; \quad V_z = \frac{-(h_O - h_A)}{t_g} \tag{10}$$

The above velocities are assumed null if $t_g = 0$. Airship objective and actual altitudes are given by h_O and h_A, respectively. The velocities as shown in Eq. (10), expressed in inertial frame, are transformed to the body reference frame through the directions cosine matrix (DCM). The desired velocities, as references for control inputs, are:

$$\begin{bmatrix} U \\ W \end{bmatrix} = \begin{bmatrix} \cos\theta\cos\psi & \cos\theta\sin\psi & -\sin\theta \\ \cos\phi\sin\theta\cos\psi + \sin\phi\sin\psi & \cos\phi\sin\theta\sin\psi - \sin\phi\cos\psi & \cos\phi\cos\theta \end{bmatrix} \begin{bmatrix} V_x \\ V_y \\ V_z \end{bmatrix} \tag{11}$$

Assuming that the control system maintains θ and ϕ values small, Eq. (11) can be simplified:

$$\begin{bmatrix} U \\ W \end{bmatrix} = \begin{bmatrix} \cos\psi & \sin\psi & -\theta \\ \theta\cos\psi + \phi\sin\psi & \theta\sin\psi - \phi\cos\psi & 1 \end{bmatrix} \begin{bmatrix} V_x \\ V_y \\ V_z \end{bmatrix} \tag{12}$$

The velocity components evaluated from Eq. 12 provide reference signals from the guidance law to the control law. The guidance law imposes the lateral angular tracking of the current to the goal aircraft point, while the reference velocities U and W determine the homing in the longitudinal plane.

Guidance in the ox_iy_i plane is controlled by the ψ_{ref} angle. An additional parameter, the Line-of-Sight (LOS) angle σ, is defined between the target interception line and the inertial axis ox_i, as shown in Fig. 3.

Aircraft linear velocity V projected in lateral-directional plane ox_iy_i is expressed as V_{ol}. The points P_{Axy} and P_{Oxy} are projections of P_A and P_O, respectively, in the same plane. Assuming some angular approximations after projections, the error angle of direction ϵ is written as:

$$\epsilon = \sigma_s - \beta - \psi \tag{13}$$

where $\sigma_s = \sigma \pm 2k\pi$ for $k \in Z$, and ψ is the current yaw angle.

Angle ϵ is assumed as the reference input to a Proportional-Integral (PI) controller (Fig. 4), that is used to attenuate its highest frequency components.

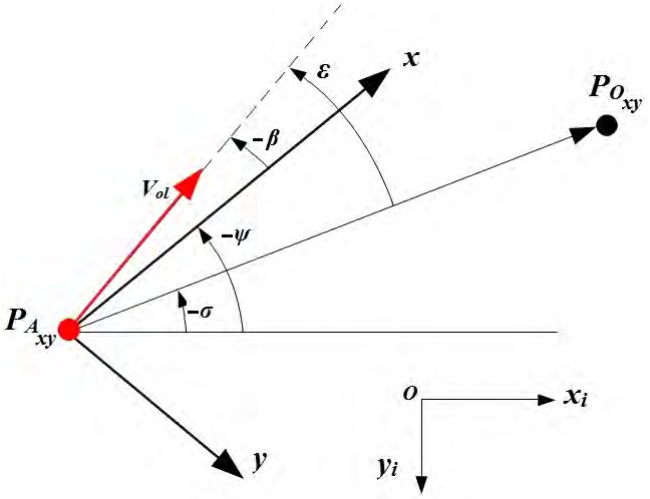

Figure 3. Lateral angles scheme.

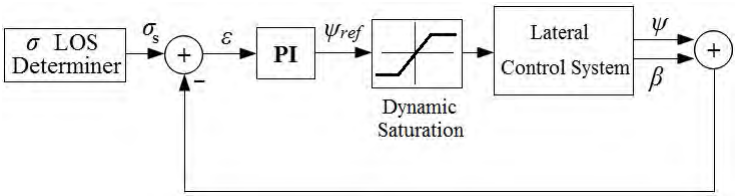

Figure 4. Diagram of lateral guidance law.

3. SYSTEMS INTEGRATION

The set of integrated systems is presented in Fig. 5. The Guidance, Navigation and Control (GNC) scheme is shown, including some navigation states to be measured or computed. At the highest level, the coverage area system provides an array of points Q, which defines a possible area to be swept. Matrix Q stores a set of $[l_i \quad \lambda_i \quad h_i]^T$ coordinates, containing latitude (l), longitude (λ) and altitude (h) data. The Path Determiner system select a sequence of feasible coordinates to be intercepted by the aircraft, in order to fulfill an optimal sweeping path. The Avionics Navigation System provides measured values of Euler angles, sideslip angle β, latitude (x_A), longitude (y_A), altitude (h_A) and calculates aircraft translational velocities U and W. Furthermore, the Path Determiner imposes the closing speed (V_c) for each new point to be intercepted. The whole process continues until all coordinates of Q are completely covered.

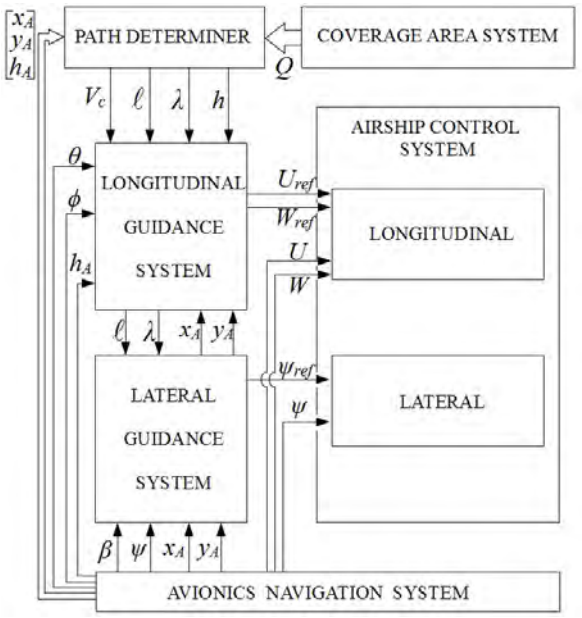

Figure 5. Block Diagram of GNC Systems.

4. HARDWARE AND FIRMWARE SYSTEMS

The Guidance, Navigation and Control (GNC) systems require a suite of devices for sensing, communications, and computing. As discussed above, navigation accuracy is increased when a Multisensor Navigation System (MNS) is used. In this project, MNS includes sonar sensors, barometer, Inertial Measurement Unit (IMU), Global Positioning System (GPS) and three-axis magnetometer. In addition, a CCD color camera is present as part of the payload. A Digital Signal Peripheral Interface Controller (dsPIC) is used for guidance and control computation, while the communication is performed through wireless Ethernet radio network.

4.1 Avionics Suite

Altimetry is performed by combining GPS, barometer and sonar range finder, which also is used to inform unexpected obstacles in the airship path. The Ultrasonic Range Finder - XL-Maxsonar EZ0 (Brainerd, MN) can provide readings from 0 to 7.65 m within 0.01 m of resolution, at 10 Hz rate. The digital barometric pressure sensor used is Bosh BMP085 (Reutlingen, Germany), that has a range of 300 to 1100 hPa with 1 Pa of resolution. The altitude can be calculated with usual international barometric formula as shown bellow:

$$H[meters] = 44330\left[1 - \left(\frac{p}{p_o}\right)^{\frac{1}{5.255}}\right] \tag{14}$$

where p is the local pressure and p_o the pressure at the sea level 1013.25hPa. Additionally, the BMP085 outputs data via I^2C protocol and performs temperature measuring with $0.1\,^{\circ}\mathrm{C}$ resolution. For measuring heading references a three-axis electronic compass (Honeywell HMC5883L, Plymouth, MN) is used, with cross axis sensitivity from milli-gauss to 8 gauss. To compute the heading angle, the body-axis components of the Earth's field hold the following relations (Kayton and Fried, 1997):

$$\begin{bmatrix} cos\psi cos\gamma \\ -sin\psi cos\gamma \\ sin\gamma \end{bmatrix} = \begin{bmatrix} A \\ B \\ C \end{bmatrix} \tag{15}$$

$$\begin{bmatrix} A \\ B \\ C \end{bmatrix} = \frac{1}{H}\begin{bmatrix} cos\theta & 0 & -sin\theta \\ 0 & 1 & 0 \\ sin\theta & 0 & cos\theta \end{bmatrix}^{-1}\begin{bmatrix} 1 & 0 & 0 \\ 0 & cos\phi & sin\phi \\ 0 & -sin\phi & cos\phi \end{bmatrix}^{-1}\begin{bmatrix} H_x \\ H_y \\ H_z \end{bmatrix} \tag{16}$$

where γ is the inclination angle of the geomagnetic field measured downwards from horizontal, H is the geomagnetic field intensity, with H_x, H_y, H_z representing components of the field in the aircraft reference frame. Finally, without being considered field contributions from aircraft's structure and electrical equipment, the heading angle can be computed as:

$$tan\psi = -\frac{B}{A} \tag{17}$$

The strapdown INS was based on the UAV Development Board version 4 (UDB4). It is designed with a dsPIC33FJ256 CPU, a MMA7361 three axis accelerometer, a dual axis IDG500 gyro and a single axis ISZ500 gyro. For real-time computing, the UDB4 16-bit 120Mhz dsPIC is used. For each axis, MMA7361 presents a sensitivity of 800 mV/g with a g-range of 1.5 g, IDG500 gyro has a maximum full-scale range of $\pm$500 °/s with 2 mV/°/s of sensitivity for x, y. For z, the ISZ500 sensor has the same sensitivity. The IMU controller is based on an open source MatrixPilot autopilot firmware (GENTLENAV, 2012). The board interface allows up to 8 input, 8 output PWM points uses an external 256Kbit EEPROM. The GPS is LS20031 (Taipei, Taiwan). It can receive up to 66 satellites, at 5 Hz rate, providing fast time-to-first-fix, one-second navigation update, and low power consumption.

Additionally, a payload camera sensor is disposed for the purpose of mock in place of the future mines identification system. The sensor consists of a DSC-6620 CCD camera (Fountain Valley, CA) with 704x480 pixel resolution, 10x optics/digital zoom and 270° pan and 90° tilt. Communication was implemented with wireless Ethernet radio network. According to the datasheet, the transmitter outputs 26 dBm of power, the antenna has a gain of 18 dBi, performing a range up to 15 Km. The signals from telemetry and payload sensor are received by a notebook in the role of land station.

4.2 Firmware

The firmware implemented in UDB4 presents some pre-defined useful routines for MatrixPilot firmware (GENTLENAV, 2012), such as Direct Cosine Matrix (DCM) computation. In fact, the UDB4 firmware is dedicated to implement a

complete autopilot for airplanes. The present work has adapted it to ASAD functionalities and control outputs with three fixed engines. Gyro signals are used as the primary source of orientation to compute DCM:

$$R = \begin{bmatrix} r_{xx} & r_{xy} & r_{xz} \\ r_{yx} & r_{yy} & r_{yz} \\ r_{zx} & r_{zy} & r_{zz} \end{bmatrix} \tag{18}$$

where relation between the DCM and Euler angles is shown in each parenthesis at right hand terms of Eq. (4-6), remembering that $(\dot{h}) = -(\dot{z})$. To obtain DCM data from gyros the following equation is used, which presents the relationship between DCM and instantaneous angular rate (Mahony *et al.*, 2008):

$$\dot{R} = R\omega^{(B)} = \omega^{(I)}R \tag{19}$$

where $\omega^{(B)}$ is the instantaneous angular rate vector of the body frame with respect to the inertial frame, as measured in body coordinates, $\omega^{(I)}$ is the same vector, but expressed in the inertial frame (Kayton and Fried, 1997) and ω is given by:

$$\omega = \begin{bmatrix} 0 & -\omega_z & \omega_y \\ \omega_z & 0 & -\omega_x \\ -\omega_y & \omega_x & 0 \end{bmatrix} \tag{20}$$

Assuming an approximation, the computing of Eq. (19), like presented by Kayton and Fried (1997), can be achieved by:

$$\dot{R} \approx \frac{R_n - R_{n-1}}{\Delta t} \approx R_{n-1}\frac{[\Delta\theta]}{\Delta t} \Rightarrow R_n \approx R_{n-1}\left([I] + [\Delta\theta]\right) \tag{21}$$

where $\Delta\theta = \omega\Delta t$ and $[I]$ is the identity matrix.

The solution of the nonlinear differential kinematic equation Eq. (21) presents drift along computing process. The source of error comes from integration, quantization, inherent gyros drift and offset. To restore DCM data some techniques are applied by the firmware. Figure 2 presents how a feedback compensator is implemented in MatrixPilot code. A more accurate angular rate data is obtained as follows:

$$\omega(t) = \omega_g(t) + \omega_c(t) \tag{22}$$

where $\omega_g(t)$ is a vector with three axis gyro measurements, and $\omega_c(t)$ is the gyro correction vector.

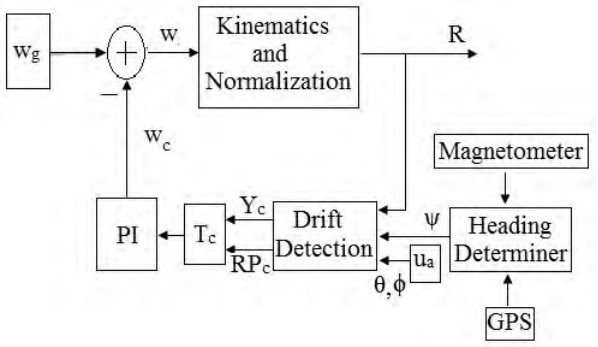

Figure 6. Adaptation of GENTLENAV (2012) Closed Loop to DCM Computation.

Primarily, the errors in DCM are minimized enforcing the orthogonality over its rows, known as *renormalization*. The orthogonality error is defined as follows:

$$\epsilon_o = \begin{bmatrix} r_{xx} & r_{xy} & r_{xz} \end{bmatrix} \begin{bmatrix} r_{yx} \\ r_{yy} \\ r_{yz} \end{bmatrix} \tag{23}$$

The error can be used to rotate the first two (X,Y) rows of R in the opposite direction by cross coupling, and then determine Z as bellow:

$$\begin{aligned} X_{orthogonal} &= \begin{bmatrix} r_{xx} \\ r_{xy} \\ r_{xz} \end{bmatrix}_{\perp} = \begin{bmatrix} r_{xx} \\ r_{xy} \\ r_{xz} \end{bmatrix} - \frac{\epsilon_o}{2}\begin{bmatrix} r_{yx} \\ r_{yy} \\ r_{yz} \end{bmatrix} \\ Y_{orthogonal} &= \begin{bmatrix} r_{yx} \\ r_{yy} \\ r_{yz} \end{bmatrix}_{\perp} = \begin{bmatrix} r_{yx} \\ r_{yy} \\ r_{yz} \end{bmatrix} - \frac{\epsilon_o}{2}\begin{bmatrix} r_{xx} \\ r_{xy} \\ r_{xz} \end{bmatrix} \\ Z_{orthogonal} &= \begin{bmatrix} r_{zx} \\ r_{zy} \\ r_{zz} \end{bmatrix}_{\perp} = X_{orthogonal} \times Y_{orthogonal} \end{aligned} \tag{24}$$

Finally, unitary norm is imposed to each row vector to keep their rotation matrix properties. Based on Taylor's series implemented in GENTLENAV (2012) the normalized equation yields:

$$\begin{aligned} X_n &= \frac{1}{2}\left(3 - X_\perp \cdot X_\perp\right) X_\perp \\ Y_n &= \frac{1}{2}\left(3 - Y_\perp \cdot Y_\perp\right) Y_\perp \\ Z_n &= \frac{1}{2}\left(3 - Z_\perp \cdot Z_\perp\right) Z_\perp \end{aligned} \tag{25}$$

where X_n, Y_n, Z_n are normalized vectors and $X_\perp$, $Y_\perp$, $Z_\perp$ are the orthonormal vectors obtained from Eq. (25).

To detect drift in computed values of the reference vector, which are caused by gyro offset, some measurements from other reference sensors must be used. Originally, UDB4 firmware is implemented using only GPS signals to yaw re-alignment. In this work, a three axis magnetometer was used to provide such a vector of reference. This brings some advantages such as enable yaw correction even at hovering flight or if the GPS data is not updated for a long period of time. The idea is using the course over ground angle direction. An indication of the yaw drift relies on angle between the course direction on the earth and the projection of x axis on the ground. The rotational correction is the Z component of the cross product between the R first column and the course over ground (COG) vector. The COG information can be obtained from GPS or by tree axis magnetometer as shown in Eq. (17).

To form a reference vector from COG angle, it is assumed that their magnitudes, in x, y inertial reference frame, are as follows:

$$\begin{aligned} C_x &= cos(\psi_m) \\ C_y &= sin(\psi_m) \end{aligned} \tag{26}$$

where ψ_m is the course over ground angle.

In the body reference system, the yaw correction can be written as:

$$Y_c = \left(r_{xx}C_y - r_{yx}C_x\right) \begin{bmatrix} r_{zx} \\ r_{zy} \\ r_{zz} \end{bmatrix} \tag{27}$$

The necessary correction for roll and pitch drifts is done from accelerometers data. The direction information is extracted using gravity data from accelerometers. Therefore, measurement of gravity in body reference frame is given as follows:

$$g_c = u_a + \omega_g \times V \tag{28}$$

where g_c presents one term that estimates the centrifugal acceleration, u_a is the accelerometers measurements vector, V is the aircraft velocity in the body reference frame, and w_g is the gyro data vector.

The cross product of the DCM z row, with the normalized gravity reference, is used to quantify the magnitude of a rotational vector correction, in the body frame:

$$RP_c = \begin{bmatrix} r_{zx} \\ r_{zy} \\ r_{zz} \end{bmatrix} \times g_c \tag{29}$$

The DCM corrections of Fig. 6 are obtained through a PI controller. The total correction is formed adding yaw and roll-pitch corrections:

$$T_c = W_1(Y_c) + W_2(RP_c) \tag{30}$$

where W_1 and W_2 are weights.

The PI controller is finally implemented by:

$$\begin{aligned} \omega_{Pc} &= K_P T_c \\ \omega_{Ic} &= \omega_{Ic} + K_I dt T_c \\ \omega_c &= \omega_{Pc} + \omega_{Ic} \end{aligned} \tag{31}$$

where K_P and K_I are, respectively, the proportional and integral gains. The choice of weights and gains depends on the compromise between accuracy and speed of recovery to disturbances (GENTLENAV, 2012).

Once DCM is computed, the Euler angles can be obtained from Eq. (18) as:

$$\begin{aligned} \theta &= -arcsin(r_{zx}) \\ \phi &= atan2(r_{zy}, r_{zz}) \\ \psi &= atan2(r_{yx}, r_{xx}) \end{aligned} \tag{32}$$

5. TESTS AND RESULTS

The ASAD-Simulator (ASAD-S) was implemented in Simulink for the nonlinear model of the aircraft with six degrees of freedom. The ASAD-S allows the assessment of various parameters and aircraft autonomous guidance in trajectories defined by waypoints. Figure 7 shows the result of the guidance and control system (GCS) for the airship performing a loitering path with Return to Launch (RTL). In the first case, with continuous blue line, constant wind of 0.2 m/ s and mild turbulent gusts for flights up to 100m of altitude were present. In the second case, with a dashed line in red, the same turbulence disturbances were applied, but the wind was increased to 0.5 m/s. In the same simulation, Figure 8 shows the expected magnitudes for roll, pitch and yaw.

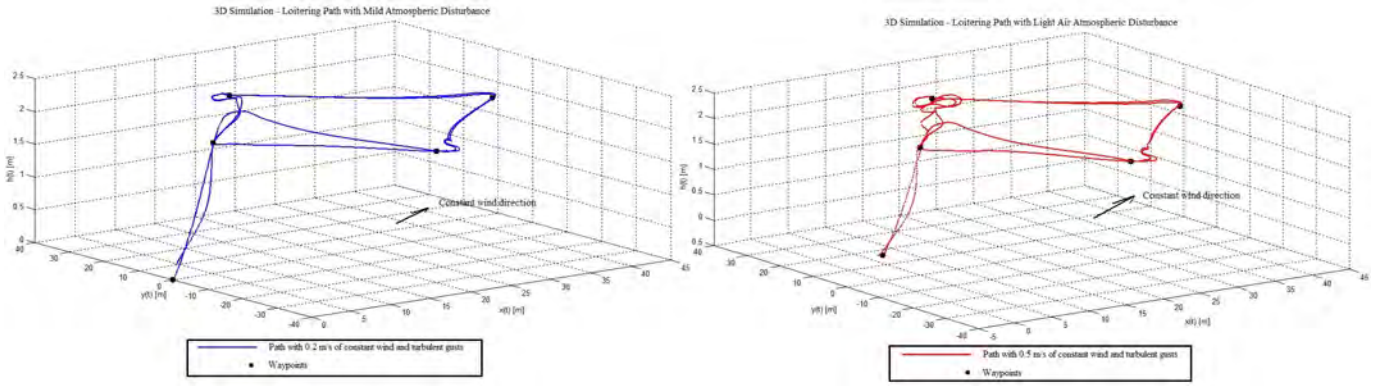

Figure 7. 3D Loitering Simulation Paths with Atmospheric Disturbances.

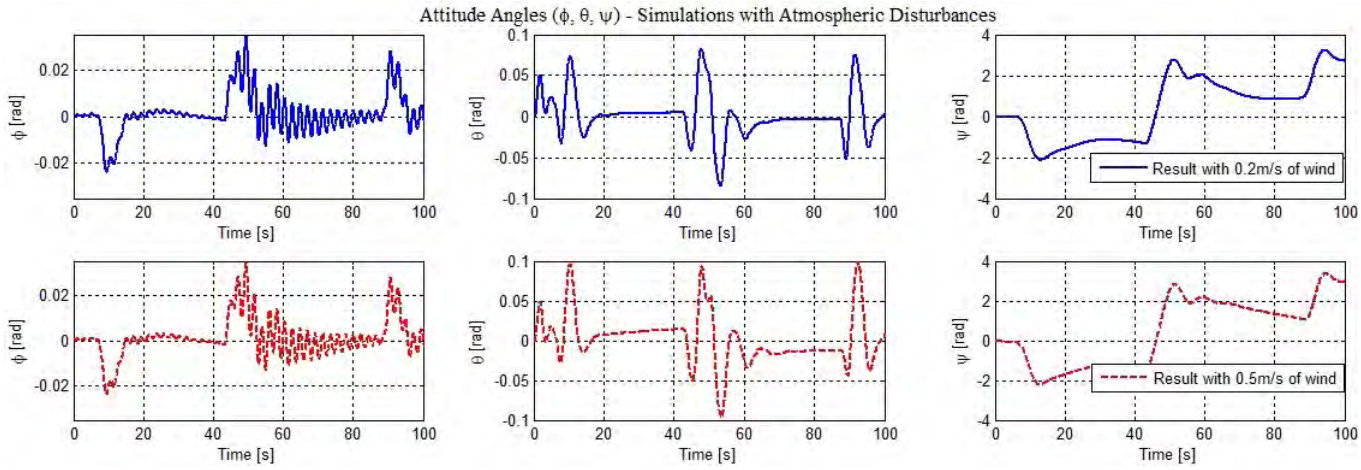

Figure 8. 3D Loitering Simulation Paths with Atmospheric Disturbances.

In some specific layout areas, for minimizing the number of half turns, helical trajectories may be required, in place of back-and-forth, to achieve coverage terrain. The altitude upwards or downwards depends on slope of the terrain in order to maintain tracking distance between the aircraft and the ground. Figure 9 shows the simulated performance of the GCS for ASAD performing in a helical path with RTL. Again, in continuous blue line, a constant wind of 0.2 m/s and mild turbulent gusts were applied. Additionally, in red dashed line the same disturbance and 0.5 m/s constant wind was simulated. Figure 10 shows the magnitudes expected for the aircraft attitude.

For all simulated situations a closing velocity of 1 m/s was assumed. Field experiments of the avionics sensors, which are currently in progress, are required before the flight tests. The avionics tests need to be performed on similar scenarios of sensor's action. For example, an area where there are underbrush and a small tree is shown in Fig. 11, together with the sonar output tracking profile. The sensor is apparently useful to detect obstacles and tracking of flight with terrain-matching navigation.

6. CONCLUSION

In this work, guidance and navigation systems for an airship with three fixed propellers are presented. The airship is expected to be used as an autonomous sweeping platform to detect landmines. The system is controlled by guidance and navigation laws outlined in this work. Additionally, the main navigation equations implemented in the firmware are

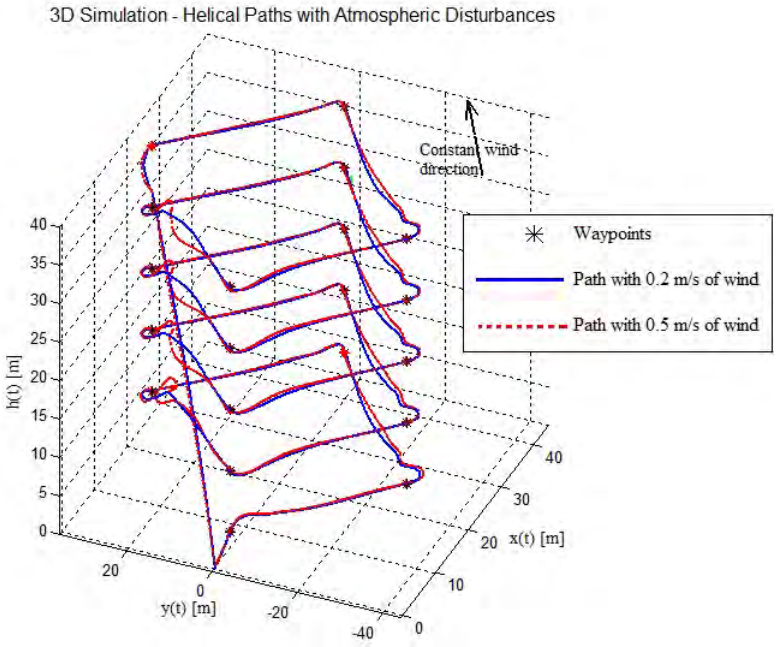

Figure 9. 3D Helical Simulation Paths with Atmospheric Disturbances.

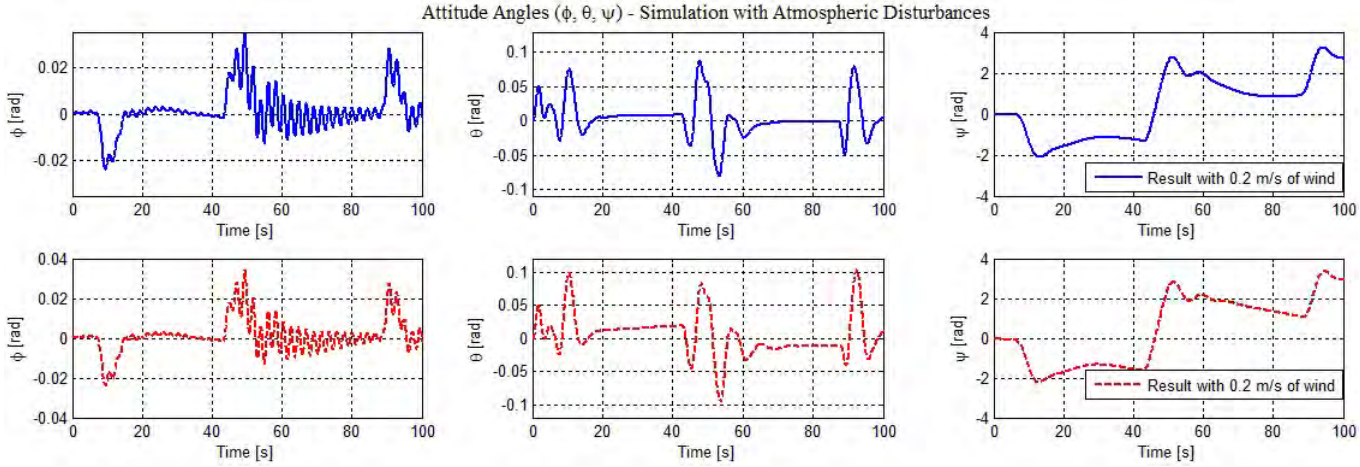

Figure 10. Attitude angles result along the helical path.

presented as well as the set of avionics sensors used. Control synthesis and its architecture are briefly commented. The concept of the overall structure for an autonomous sweeping system is also presented. The guidance system proposed can control velocities and altitude in the longitudinal plane and heading in the lateral plane. As experimental preliminary results, altimetry sonar signal, in a typical application scenario, is shown, as well as a waypoint tracking simulations in presence of wind and turbulence gusts.

7. ACKNOWLEDGEMENTS

The authors acknowledge the Brazilian Army, CAPES, FAPERJ and CNPq for institutional and financial support.

8. REFERENCES

Adamski, W., Herman, P., Bestaoui, Y. and Kozlowski, K., 2010. "Control of airship in case of unpredictable environment conditions". *Conference on Control and Fault Tolerant Systems*, pp. 843–848, Nice.

Allen, H.J. and Perkins, E. W., 1951. "Characteristics of flow over inclined bodies of revolution". *NACA RM A50L07*.

Azinheira, J. R., Moutinho, A. and Paiva, E.C., 2006. "Airship hover stabilization using a backstepping control approach". *Journal of Guidance, Control and Dynamics, AIAA*, Vol. 29, No. 4, pp. 903–914.

Azinheira, J. R., Moutinho, A. and Paiva, E.C., 2008. "Erratum on influence of wind speed on airship dynamics". *Journal of Guidance, Control and Dynamics, AIAA*, Vol. 31, No. 2, pp. 443–444.

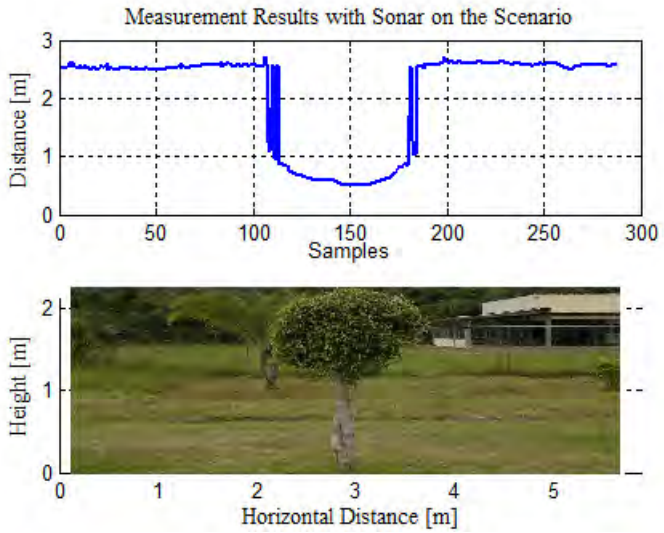

Figure 11. Test of Close Range Altitude Sensor (Sonar) - Scenario with Typical Obstacles.

Azinheira, J. R., Paiva, E.C. and Bueno, S.S., 2002. "Influence of wind speed on airship dynamics". *Journal of Guidance, Control and Dynamics, AIAA*, Vol. 25, No. 6, pp. 1116–1124.

Azinheira, J. R., Paiva, E.C., Carvalho, J.R.H., Ramos,J.J.G., Bueno, S.S., Bergerman, M. and Ferreira, P.A.V., 2001. "Lateral/directional control for an autonomous, unmanned airship". *Aircraft Engineering and Aerospace Technology*, Vol. 73, Issue 5, pp. 453–459.

Azinheira, J. R., Paiva, E.C., Ramos, J.J.G. and Bueno, S.S., 2000. "Mission path following for an autonomous unmanned airship". *International Conference on Robotics and Automation, IEEE*, Vol. 2, pp. 1269–1275, San Francisco.

Bishop, P.K., Perry, K.M. and Poulter, M.A., 1998. "Airborne minefield detection". In *Second International Conference on Detection of Abandoned Land Mines, IEEE*. Edinburgh, UK.

Burgess, C.P., 1927. *Airship Design*. Roland Press, New York.

Cross, E. and Osborn, S., 2010. "Aircraft mounted ground penetrating synthetic aperture radar". In *International Symposium "Humanitarian Demining 2010", HCR-CTRO*. Šibenik, Croatia.

Daniels, D.J., 2006. "A review of GPR for landmine detection". *Sensing and Imaging: An International Journal*, Vol. 7, pp. 90–123.

do Valle, R.C., Menegaldo, L.L. and Simões, A.M., 2012. "Longitudinal control of a robotic airship with three thrusters". In *Brazilian Conference on Automation (CBA)*. Campina Grande, Brazil.

Earon, E.J.P., Rabbath, C.A. and Apkarian, J., 2007. "Design and control of a novel hybrid vehicle concept". *In AIAA Guidance, Navigation, and Control Conference and Exhibit*, Hilton Head.

Elfes, A., Bueno, S.S., Bergerman, M., Paiva, E.C., Ramos, J.J.G. and Azinheira, J.R., 2003. "Robotic airships for exploration of planetary bodies with an atmosphere: Autonomy challenges". *Journal of Autonomous Robots*, Vol. 14, pp. 147–164.

Frye, M.T., Gammon, S.M. and Qian, C., 2007. "The 6-DOF dynamic model and simulation of the tri-turbofan remote-controlled airship". In *Proceedings of American Control Conference, IEEE*. New York.

GENTLENAV, 2012. "Firmware for Bill Premerlani's IMU based UAV dev board autopilots". 11 Jun. 2013 <http://code.google.com/p/gentlenav/>.

Gomes, S.B.V. and Ramos, J.J.G., 1998. "Airship dynamic modeling for autonomous operation". In *International Conference on Robotics and Automation, IEEE*, Vol. 4, pp. 3462–3467, Leuven, Belgium.

Hoerner, S.F., 1958. *Fluid-dynamic drag: Practical Information on Aerodynamic Drag and Hydrodynamic Resistance*. Self-Published, Midland Park, New Jersey.

Huang, Z.J. and Fang, J.C., 2005. "Integration of MEMS inertial sensor-based GNC of a UAV". *International Journal of Integration Technology*, Vol. 11, pp. 123–132.

Jiong, Y., Lei, Z., Jiangping, D., Rong, S. and Jianyu, W., 2010. "GPS/SINS/BARO integrated navigation system for UAV". In *2010 International Forum on Information Technology and Applications, IEEE*. Kunming, China.

Kayton, M. and Fried, W.R., 1997. *Avionics Navigation Systems*. John Wiley & Sons, INC, New York, 2nd edition.

Khoury, G.A. and Gillett, J.D., 1999. *Airship Technology*. Cambridge University Press, England, UK, 2nd edition.

Kulczycki, E.A., Johnson, J.R., Bayard, D.S., Elfes, A. and Quadrelli, M.B., 2008. "On the development of parameterized linear analytical longitudinal airship models". In *AIAA Guidance, Navigation and Control Conference*. Honolulu.

Kulczycki, E.A., Joshi, S.S, Hess, R.A and Elfes, A., 2006. "Towards controller design for autonomous airships using

SLC and LQR methods". In *Guidance, Navigation, and Control Conference and Exhibit, AIAA*. Keystone.

Lamb, H., 1945. *Hydrodynamics*. Dover, New York, 6th edition.

Li, Y., 2008. "Dynamics Modeling and Simulation of Flexible Airship". In *PhD Thesis, Department of Mechanical Engineering, McGill Univ.*, Montreal.

Li, Y. and Nahom, M., 2007. "Modeling and simulation of airship dynamics.". In *Journal of Guidance, Control and Dynamics, AIAA*, Vol. 30, No. 6, pp. 1691–1700.

Li, Y., Nahom, M. and Sharf, I., 2011. "Airship dynamics modeling: A literature review". In *Progress in Aerospace Sciences, Elsevier*, Vol. 47, Issue 3, pp. 217–239.

Liang, W.X. and Xiong, S.X., 2006. "Airship attitude tracking system". In *Applied Mathematics and Mechanics*, Vol. 27, Issue 7, pp. 919–926.

Liesk, T., 2012. "Control Design and Validation for an Unmanned, Finless Airship". In *PhD Thesis, Department of Mechanical Engineering, McGill Univ.*, Montreal.

Lin, C.F., 1991. *Modeling-Design-Analysis-Simulation-Evaluation (MDASE) of NGC Processing*. Prentice-Hall, New Jersey, 1st edition.

MacDonald, J. and Lockwood, J.R., 2003. *Alternatives for Landmine Detection*. RAND Corporation, Santa Monica.

Mahony, R., Hamel, T. and Pflimlin, J.M., 2008. "Nonlinear complementary filters on the special orthogonal group". *IEEE Transactions on Automatic Control*, Vol. 53, pp. 1203–1218.

McLean, D., 1990. *Automatic Flight Control Systems*. Prentice Hall, England, UK, 1st edition.

Meurer, H., Wehner, M., Schillberg, S., H.-Rinke, K., Kühn, C., Raven, N. and Wirtz, T., 2010. "An emerging remote sensing technology and its potential impact on mine action". In *International Symposium "Humanitarian Demining 2010", HCR-CTRO*. Šibenik, Croatia.

Mueller, J.B., Paluszek, J.B. and Zhao, Y.J., 2004. "Development of an aerodynamic model and control law design for a high altitude airship". In *AIAA 3rd "Unmanned Unlimited" Technical Conference, Workshop and Exhibit*. Chicago.

Munk, M.M., 1922. "Notes on aerodynamic forces - III: The aerodynamic forces on airships". *NACA TN 106*.

Munk, M.M., 1924. "Some tables of the factors of apparent additional mass.". *NACA TR 197*.

Munk, M.M., 1936. "Aerodynamics of airships.". *Aerodynamics Theory, 6*.

Nong, Y., 2012. "Design of Small Highly Maneuverable Airships". In *Master of Engineering Thesis, Department of Mechanical Engineering, McGill Univ.*, Montreal.

Paiva, E.C., Azinheira, J.R., Ramos, J.J.G., Moutinho, A. and Bueno, S.S., 2006. "Project Aurora: Infrastructure and flight control experiments for a robotic airship". *Journal of Field Robotics*, Vol. 23, pp. 201–222.

Paiva, E.C., Bueno, S.S., Gomes, S.B.V., Ramos, J.J.G. and Bergerman, M., 1999. "A control system development environment for Aurora's semi-autonomous robotic airship". *International Conference on Robotics and Automation, IEEE*, Vol. 3, pp. 2328–2335, Detroit.

Paiva, E.C., Carvalho, J.R.H., Ferreira, P.A.V. and Azinheira, J. R., 2001. "An H_2/H_∞ PID heading controller for Aurora-I semi-autonomous robotic airship". *In 14th Lighter-Than-Air-Systems Technology Conference* , Ohio.

Peddiraju, P., 2010. "Development and validation of a dynamics model for an unmanned, finless airship". In *Master's thesis, Department of Mechanical Engineering, McGill Univ.*, Montreal.

Ramos, J.J.G., Paiva, E.C., Azinheira, J.R., Maeta, S.M., Mirisola, L.G.B, Bergerman, M. and Faria, B.G., 2001. "Autonomous flight experiment with a robotic unmanned airship". *International Conference on Robotics and Automation, IEEE*, Vol. 4, pp. 4152–4157.

Repoulias, F. and Papadopoulos, E., 2008. "Robotic airship trajectory tracking control using a backstepping methodology". In *International Conference on Robotics and Automation, IEEE*, pp. 188–193, Pasadena.

Silveira, G.F, Carvalho, J.R.H, Rives, P., Azinheira, J. R., Bueno, S.S. and Madrid, M.K., 2002. "Optimal visual servoed guidance of outdoor autonomous robotic airships". *Proceedings in American Control Conference*, Vol. 1, pp. 779–784.

Simões, A.M., Apkarian, P. and Noll, D., 2009. "Nonsmooth multi-objective synthesis with applications". *Control Engineering Practice, Elsevier*, Vol. 17, pp. 1338–1348.

Thomasson, P. G., 2000. "Equations of motion of a vehicle in a moving fluid". In *Journal of Aircraft, AIAA*, Vol. 37, No. 4, pp. 630–639.

Wang, X., Y-Ma and Shan, X., 2010. "Modeling of stratosphere airship". In *2010 3rd International Symposium on Systems and Control in Aeronautics and Astronautics*. Harbin, China.

Wimmer, D.A. and Well, K.H., 2001. "Instrumentation, identification and control of airship "Lotte"". In *International Conference on Robotics and Automation, IEEE*, Vol. 4, pp. 3462–3467, Leuven, Belgium.

Zhang, Y., Qu, W.D., Xi, Y.G. and Cai, Z.L., 2008. "Adaptive stabilization and trajectory tracking of airship with neutral buoyancy". In *ACTA Automatica Sinica*, Vol. 34, No. 11, pp. 1437–1440.

9. RESPONSIBILITY NOTICE

The authors are the only responsible for the printed material included in this paper.